



## Article

# Magnetite nanoparticles are metastable biogeobatteries in consecutive redox cycles driven by microbial Fe oxidation and reduction

T. Bayer<sup>1</sup>, N. Jakus<sup>1,†</sup> , A. Kappler<sup>1,2</sup>  and J. M. Byrne<sup>3</sup> 

<sup>1</sup>Geomicrobiology Group, Department of Geosciences, University of Tuebingen, Schnarrenbergstrasse 94-96, 72076 Tuebingen, Germany; <sup>†</sup>Current address: Environmental Microbiology Laboratory, École Polytechnique Fédérale de Lausanne, CE1 644, Lausanne CH 1015, Switzerland; <sup>2</sup>Cluster of Excellence: EXC 2124: Controlling Microbes to Fight Infection, Auf der Morgenstelle 28D, 72076 Tuebingen, Germany and <sup>3</sup>School of Earth Sciences, University of Bristol, Queens Road BS8 1RJ, Bristol, UK

## Abstract

Iron (Fe) minerals play a crucial role in biogeochemical cycles due to their ubiquity in nature, high adsorption capacity and redox activity towards many other elements. Mixed-valent Fe minerals are unique since they contain Fe(II) and Fe(III). For example, magnetite (Fe(II)Fe(III)<sub>2</sub>O<sub>4</sub>) nanoparticles (MNPs) can affect the availability and mobility of nutrients and contaminants. This is due to the high surface area to volume ratio and the presence of Fe(II) and Fe(III), allowing redox transformation of (in-)organic contaminants. Recent studies have shown that magnetite can serve as an electron source and sink for Fe(II)-oxidizing and Fe(III)-reducing microorganisms, storing and releasing electrons; thus, it functions as a biogeobattery. However, the ability of MNPs to act as biogeobatteries over consecutive redox cycles and the consequences for mineral integrity and identity remain unknown. Here, we show MNPs working as biogeobatteries in two consecutive redox cycles over 41 days. MNPs were first oxidized by the autotrophic nitrate-reducing Fe(II)-oxidizing culture KS and subsequently reduced by the Fe(III)-reducing *Geobacter sulfurreducens*. In addition to reduced magnetite, we identified the Fe(II) mineral vivianite after reductions, suggesting partial reductive dissolution of MNPs and re-crystallization of Fe<sup>2+</sup> with phosphate from the growth medium. Measurements of the Fe(II)/Fe(III) ratio revealed microbial oxidation and reduction for both the first redox cycle (oxidation: 0.29±0.014, reduction: 0.75±0.023) and the second redox cycle (oxidation: 0.30±0.015, reduction: 1.64±0.10). Relative changes in magnetic susceptibility ( $\Delta\kappa$  in %) revealed greater changes for the second oxidation (−8.7±1.99%) than the first (−3.9±0.19%) but more minor changes for the second reduction (+14.29±0.39%) compared to the first (+25.42±1.31%). Our results suggest that MNPs served as biogeobatteries but became less stable over time, which has significant consequences for associated contaminants, nutrients and bioavailability for Fe-metabolizing microorganisms.

**Keywords:** magnetite; nanoparticles; iron oxidation; iron reduction; dissolution; biogeobattery

(Received 22 November 2023; revised 01 March 2024; manuscript accepted: 07 May 2024)

## Introduction

Biogeochemical element cycles determine the distribution and availability of nutrients and contaminants in environmental systems. Iron (Fe) (oxyhydr)oxides are essential constituents in sediments and soils as Fe is one of the most abundant elements in Earth's crust (Kendall, Anbar, Kappler and Konhauser, 2012) and is interlinked with the global carbon, nitrogen and oxygen cycles (Kappler, Becker and Enright, 2021). Fe is present in ferrous Fe(II) and ferric Fe(III) forms (Kappler, Bryce, Mansor, Lueder, Byrne and Swanner, 2021). As Fe is critical to almost all living organisms as a nutrient, it has a high turnover in the biosphere (Kappler and Straub, 2005) and can undergo redox cycling between

oxidation states by abiotic or biotic processes (Kappler, Becker and Enright, 2021; Kappler, Bryce, Mansor, Lueder, Byrne and Swanner, 2021). At circumneutral pH, Fe(II) can be oxidized by photoautotrophic nitrate-reducing or by microaerophilic bacteria (Widdel, Schnell, Heising, Ehrenreich, Assmus and Schink, 1993; Straub, Benz, Schink and Widdel, 1996; Emerson and Moyer, 1997; Bryce *et al.*, 2018). Fe(III)-reducing bacteria use fatty acids or H<sub>2</sub> as electron donors to reduce Fe(III) in anoxic conditions (Lies, Hernandez, Kappler, Mielke, Gralnick and Newman, 2005; Lovley *et al.*, 2011). Mixed-valent Fe minerals are unique because they contain both Fe(II) and Fe(III) in their crystal structure (Usman, Byrne, Chaudhary, Orsetti, Hanna, Ruby, Kappler and Haderlein, 2018). Magnetite, an abundant mixed-valent Fe oxide (Maher and Taylor, 1988; Evans and Heller, 2003), contains two Fe(III) and one Fe(II) per unit cell in crystals with ideal stoichiometry, giving it the formula Fe(II)Fe(III)<sub>2</sub>O<sub>4</sub>. While Fe(III) in magnetite is present in octahedral or tetrahedral coordination, Fe(II) is only in tetrahedral coordination. In the environment, magnetite can be formed

**Corresponding author:** James M. Byrne; Email: james.byrne@bristol.ac.uk

**Cite this article:** Bayer T., Jakus N., Kappler A., & Byrne J.M. (2024). Magnetite nanoparticles are metastable biogeobatteries in consecutive redox cycles driven by microbial Fe oxidation and reduction. *Geo-Bio Interfaces* 1, e3, 1–11.  
<https://doi.org/10.1180/gbi.2024.2>

through biological processes such as microbial Fe(II) oxidation (Miot, Li, Benzerara, Sougrati, Ona-Nguema, Bernard, Jumas and Guyot, 2014), microbial Fe(III) reduction (Lovley, Stolz, Nord Jr and Phillips, 1987; Kappler, Thompson and Mansor, 2023) and intracellularly by magnetotactic bacteria (Schüler, 2002; Uebe and Schüler, 2016; Amor, Tharaud, Gélabert and Komeili, 2020), which use magnetite crystals to navigate along the Earth's magnetic field (Byrne and Amor, 2023). Abiotic processes that produce magnetite include weathering (Evans and Heller, 2003) and anthropogenic processes such as combustion (Maher, 2009). When present as nanoparticles (MNPs), magnetite can have a specific surface area of up to  $100 \text{ m}^2 \text{ g}^{-1}$  (Cornell and Schwertmann, 2003; Bayer, Wei, Kappler and Byrne, 2023), which promotes interactions with nutrients and contaminants via adsorption (Sundman, Vitzhum, Adaktylos-Surber, Figueroa, van der Laan, Daus, Kappler and Byrne, 2020; Bayer, Wei, Kappler and Byrne, 2023) or redox reactions (Peterson, White, Brown and Parks, 1997). These interactions are heavily influenced by the Fe(II)/Fe(III) ratio, as it changes the redox properties, surface charge, magnetic properties and, hence, the reactive surface of the mineral (Gorski, Nurmi, Tratnyek, Hofstetter and Scherer, 2010). Since there are two Fe(III) for every Fe(II), the Fe(II)/Fe(III) ratio for stoichiometric magnetite is 0.5. Maghemite ( $\gamma\text{-Fe}_2\text{O}_3$ ) is the fully oxidized end member of magnetite with a deficiency in Fe to maintain charge balance (Usman, Byrne, Chaudhary, Orsetti, Hanna, Ruby, Kappler and Haderlein, 2018). It was previously shown that the ratio of MNPs can exceed the stoichiometry ( $\geq 0.5$ ), particularly following microbial Fe(III) reduction (Byrne, Klueglein, Pearce, Rosso, Appel and Kappler, 2015; Bayer, Wei, Kappler and Byrne, 2023), as it was demonstrated that the Fe(II)/Fe(III) ratio can be altered through activity of Fe-metabolizing microorganisms. Fe(II) in MNPs was shown to be an electron source for the phototrophic Fe(II)-oxidizing strain *Rhodospseudomonas palustris* TIE-1 and Fe(III) as an electron sink for the Fe(III)-reducing *Geobacter sulfurreducens* and magnetite was, therefore, classified as a biogeobattery (Byrne, Klueglein, Pearce, Rosso, Appel and Kappler, 2015). Additionally, magnetite particles can play a crucial role in long-range electron transport (Liu, Rotaru, Shrestha, Malvankar, Nevin and Lovley, 2015; Byrne *et al.*, 2016). During these previous experiments, the MNP-biogeobattery capabilities (that is, the capability to serve as electron donor and acceptor for microbial metabolisms) were mainly tested with cell suspension experiments (high cell density of added microorganisms) in comparatively short time frames. Therefore, long-term effects and interactions between MNPs and microbes in consecutive cycles were not fully explored. We expect that consecutive redox cycles with lower numbers of added microorganisms have key effects on the stability and stoichiometry of MNPs and, hence, on the redox and magnetic properties. It was previously demonstrated that long-term incubations could reveal previously overlooked processes during Fe(II) oxidation (Bayer, Tomaszewski, Bryce, Kappler and Byrne, 2023). Therefore, to shed light on the importance of prolonged microbial Fe(II) oxidation and Fe(III) reduction on the properties of MNPs, long-term experiments with growing cultures (low volumes of added microbes) are key to understanding changes to MNPs properties, which will influence the (bio-)availability of contaminants and nutrients in natural environments. In this study, we investigated microbial oxidation and reduction of MNPs over 41 days by the nitrate-reducing Fe(II)-oxidizing culture KS and Fe(III)-reducing *G. sulfurreducens*. We quantified the Fe(II)/Fe(III) ratio and the relative change in magnetic susceptibility  $\Delta\kappa$  in % during two full redox cycles driven by these microorganisms. Additionally, we analysed mineral

properties, composition and morphology by X-ray diffractometry ( $\mu\text{XRD}$ ), Mössbauer spectroscopy, scanning electron microscopy (SEM) and Fourier-transform infrared spectroscopy (FTIR).

## Experimental Methods

### Magnetite synthesis

Magnetite nanoparticles were synthesized using a modified version of Pearce *et al.* (Pearce, Qafoku, Liu, Arenholz, Heald, Kukkadapu, Gorski, Henderson and Rosso, 2012). Specifically, a separating funnel was kept anoxic by sealing it with a rubber stopper and continuously flushing it with  $\text{N}_2$  in a fume hood. The funnel was connected to a rubber-stopper-sealed 1 L Schott bottle via rubber tubing. To ensure anoxia of the system, it was flushed for  $\geq 5$  min after adding anoxic Fe solution to the Schott bottle and an anoxic  $\text{NH}_4\text{OH}$  solution to the separating funnel. The synthesized magnetite was collected and washed four times with anoxic ultrapure water and then resuspended in a pH 7 bicarbonate ( $\text{NaHCO}_3$ ) buffer (22 mM).

### Cultivation of microorganisms

The nitrate-reducing Fe(II)-oxidizing culture KS and the Fe(III)-reducing *G. sulfurreducens* were obtained from the culture collection of the Geomicrobiology group at the University of Tuebingen. Cells were cultivated before inoculation for seven days (culture KS) or five days (*G. sulfurreducens*) in replicate 50 ml serum bottles with a volume of 25 ml and 10% v/v inoculum. As previously described, incubations were performed in a bicarbonate-buffered medium (Tominski, Heyer, Lösekann-Behrens, Behrens and Kappler, 2018). Once fully grown, the bottles from each respective culture were pooled in a sterile, anoxic Schott bottle to ensure homogeneity. For culture KS, 4 mM of  $\text{NaNO}_3$ , and for *G. sulfurreducens*, 20 mM of Na-acetate was added from sterile and anoxic stock solutions.

### Experimental setup

Large volume 9 x 1 L Schott bottles and small volume 9 x 50 ml serum bottles (six replicates and three controls each) were amended with a bicarbonate buffered growth medium, 30 mM magnetite (as total Fe concentration) and 4 mM  $\text{NaNO}_3$ . Culture KS (10% v/v) was added to six bottles, while the same volume of buffered medium was added to three controls. The total volumes were 850 ml and 25 ml, respectively. Schott bottles were sealed with a rubber stopper and a regular lid with an opening that allowed sampling. Serum bottles were sealed with a rubber stopper and a heat-shrinking tube to avoid interferences of otherwise commonly used aluminium lids during magnetic susceptibility measurements (Porsch, Dippon, Rijal, Appel and Kappler, 2010). Large Schott bottles were sampled for geochemical and mineralogical analysis while the smaller serum bottles were mainly used for magnetic susceptibility measurements. To ensure consistency with the larger Schott bottles, serum bottles were irregularly sampled for geochemical analysis. An overview of the sampling procedure is displayed in Fig. S1.

### Oxidation and reduction cycles

At the end of each redox half-cycle MNPs were washed five times with an anoxic and sterile bicarbonate buffer to remove cells. To retain MNPs in the bottles, two strong magnets were applied from the bottom and the side before and during the disposal of the

washing solution. The bottles were kept anoxic through a constant stream of  $N_2/CO_2$  gas, and sterile by working next to Bunsen burners. After washing, new growth medium was added to the MNPs, followed by vigorous shaking to guarantee thorough mixing. Microorganisms and stock solutions ( $NaNO_3/Na$ -acetate) were added to achieve consistent volumes and concentrations of  $NaNO_3/Na$ -acetate and 10% v/v inoculum of the respective bacteria.

### Geochemical analyses

Samples for geochemical analyses were taken in the glove box, centrifuged for five minutes at 10,000 g and split into pellet and supernatant. The pellet was dissolved in the glove box in 40 mM sulfamic acid in 6 M HCl (60 min) (Klueglein and Kappler, 2013; Schaedler, Kappler and Schmidt, 2017). The supernatant was used to quantify dissolved Fe, nitrate and acetate (see Fig. S2 for nitrate and acetate). The 6 M HCl extract was diluted with 1 M HCl, and the Fe concentrations were determined via the ferrozine assay (Stookey, 1970). Fe(III) was calculated as the difference between measurements for total Fe and Fe(II). This sampling was performed daily for Schott bottles. For the 50 ml serum bottles, it was performed exclusively before the first and after the last magnetic susceptibility measurement of each redox phase.

### Magnetic susceptibility $\kappa$ measurements

In-situ volume-specific magnetic susceptibility  $\kappa$  was measured with a KLY-3 Kappabridge (AGICO, Czech Republic). The 50 ml serum bottles were lowered into a coil and the response to an applied magnetic field (peak magnetic field of 300 A/m and a frequency of 875 Hz) was measured. Each bottle of biological and control replicates was measured in triplicate.

### $^{57}Fe$ Mössbauer spectroscopy

Samples were taken for Mössbauer spectroscopy before the addition of bacteria, after the addition of culture KS, at the end of the first oxidation and after each subsequent redox half phase. In the glove box, 12 ml liquid was filtered through a 0.45  $\mu m$  pore-size syringe filter (Millipore membrane); filtered minerals were embedded in Kapton tape and stored at  $-20^\circ C$  until measurement. The samples were inserted into a closed-cycle exchange gas cryostat (SHI-650-5; Janis Research, USA). Spectra were collected at 140 K using a constant acceleration drive system (WissEI, Blieskastel, Germany). Gamma radiation was emitted by a  $^{57}Co$ -source embedded in a rhodium matrix. Spectra were calibrated against a 7- $\mu m$ -thick Fe(0) foil at room temperature. Recoil (University of Ottawa, Canada) was used to fit spectra using the extended Voigt-based fitting model (xVBF). The Lorentzian half-width-half-maximum (HWHM) value was kept constant at either 0.124 mm/s or 0.140 mm/s as two separate Mössbauer instruments were used for sample analyses, each with different instrumental broadening. Spectra were analysed with respect to the isomer shift ( $\delta$ ), quadrupole splitting ( $\Delta E_Q$ ) and hyperfine magnetic field ( $B_{hf}$ ).

### X-ray diffractometry (XRD)

In an anoxic glove box, samples for  $\mu XRD$  analysis were collected from batch incubations. Solid precipitates were washed with anoxic

Milli-Q and dried and stored in Eppendorf tubes in an oven ( $28^\circ C$ ).  $\mu XRD$  was performed using Bruker's D8 Discover GADDS XRD2 micro-diffractometer equipped with a standard sealed tube with a Co-anode (CoK $\alpha$  radiation,  $\lambda = 0.17903$  nm, 30 kV/30 mA). The measurement time was 120 s at two detector positions ( $15^\circ$  and  $40^\circ$ ). The resulting diffractograms were analysed using the software Match! (version 3.6.2.121) using reference patterns from the Crystallography Open Database (ver. COD-Inorg REV248644 2020.03.03). Before starting the measurement, samples were retained in an  $N_2$ -filled Schott bottle for as long as possible to prevent oxidation. The average crystal size (nm) and the lattice parameter (ang) were calculated from the  $\mu XRD$  patterns by analysis of the most intense reflection of magnetite (311) at 2 Theta of  $43.36^\circ$  (Patterson, 1939).

### Scanning electron microscopy

Samples for scanning electron microscopy (SEM) were prepared at the end of the second reduction: 2 ml samples were removed from different bottles with a syringe and needle in an anoxic glove box, washed with Milli-Q water and then carefully distributed on a glass slide covered with 0.1% w/v aqueous solution of Poly-L-Lysine to provide a hydrophilic surface for cells. After drying in the glove box, the samples were transported in an  $N_2$ -filled Tupperware box to be coated with a Bal-Tec SCD005 sputter coater to prevent as much contact with  $O_2$  as possible. Samples were coated with platinum for 120 s at  $4 \times 10^{-2}$  mbar, 30 mA and a working distance of 35 mm, which yielded a platinum layer of 12 nm thickness. SEM was performed with a ZEISS Crossbeam 550L, an acceleration voltage of 5 kV and the SESI (Secondary electrons Secondary ions) detector.

### Fluorescence microscopy

Culture KS collected after the first oxidation was imaged between repeated washing steps to determine the number of washes needed to remove bacterial cells: 10  $\mu L$  of the sample were stained with 2  $\mu L$  of Dead/Live stain to obtain a fluorescence signal (LIVE/DEAD BacLight bacterial viability kit, Molecular Probes) and investigated with a Leica DM 5500 B (Leica Microsystems).

### Specific surface area determination

To determine the specific surface area (SSA), MNPs were freeze-dried and weighed out anoxically. For SSA determination, a Micromeritics Gemini VII surface area and porosity analyser (Micromeritics Instrument Cooperation, USA) equipped with a VacPrep 061 using  $N_2$  as adsorbate, was used.

### Infrared spectroscopy

Samples for Fourier-transformed infrared (FTIR) analysis were collected after the second oxidation and the second reduction. Samples were washed with anoxic MilliQ water and dried in Eppendorf tubes in an anoxic glove box. Spectra were collected on a Bruker Vertex 70 FTIR spectrometer equipped with a deuterated triglycine sulfate (DTGS) detector (Bruker Optics, Inc., Ettlingen, Germany). Pellets were prepared by mixing 1 mg of the sample with 250 mg of KBr (spectrometry grade) and pressed into a pellet. Spectra were collected under a vacuum from 400 to 4000  $cm^{-1}$  for an average of 256 scans at an instrument resolution of 4  $cm^{-1}$  (Wan, Yan, Liu, Tan, Chen and Feng, 2016).



## Results & Discussion

### MNPs characterization

The MNPs were analysed using a range of analytical techniques. BET measurements revealed a specific surface area of freeze-dried unaltered MNPs of  $90.3 \text{ m}^2\text{g}^{-1}$ . The Fe(II)/Fe(III) ratio of MNPs (Fe(II)/Fe(III)<sub>mag</sub> hereafter) before inoculation was determined with the ferrozine assay as  $0.43 \pm 0.002$ . Both values closely agree with earlier studies (Pearce, Qafoku, Liu, Arenholz, Heald, Kukkadapu, Gorski, Henderson and Rosso, 2012; Bayer, Wei, Kappler and Byrne, 2023).  $^{57}\text{Fe}$  Mössbauer spectroscopy of an MNP sample before inoculation revealed pure magnetite with two characteristic sextets corresponding to octahedrally and tetrahedrally coordinated Fe (Fig. S3, light blue and grey). Analysis of the relative spectral areas of the two sextets resulted in a Fe(II)/Fe(III)<sub>mag</sub> of  $0.45 \pm 0.01$  (Table S1) (Gorski and Scherer, 2010), which is in good agreement with the ferrozine measurement. The average crystallite size of our MNPs from  $\mu\text{XRD}$  patterns was calculated to be 10.24 nm (Patterson, 1939; Klug and Alexander, 1974) and the Fe(II)/Fe(III)<sub>mag</sub> from  $\mu\text{XRD}$  data was calculated as 0.52 (Table S1) (Pearce, Qafoku, Liu, Arenholz, Heald, Kukkadapu, Gorski, Henderson and Rosso, 2012). Partial adsorption of reduced Fe(II) to the inner surface of the utilized glassware is a possible explanation for inconsistent results between chemical and spectroscopic methods, especially towards the later stages of the experiment (Notini, Byrne, Tomaszewski, Latta, Zhou, Scherer and Kappler, 2019; Dong et al., 2020).

### Measurements of the Fe(II)/Fe(III) ratio and magnetic susceptibility $\kappa$ during redox cycling experiment

Measurements of the Fe(II)/Fe(III) ratio (Fe(II)/Fe(III)<sub>total</sub> hereafter) by ferrozine during the redox cycling experiments (Fig. 1a) showed that the MNPs were successfully oxidized by culture KS, as previously described for this strain (Bayer, Wei, Kappler and Byrne, 2023).

Initially ( $t = 0$ ), the Fe(II)/Fe(III)<sub>total</sub> determined by ferrozine seemed lower than expected for stoichiometric magnetite ( $0.404 \pm 0.005$  for the experiments and  $0.434 \pm 0.001$  for controls). Stoichiometric magnetite is expected to have a Fe(II)/Fe(III) ratio of 0.5. However, slightly lower values have previously been seen for MNPs synthesized using this method (Byrne, Klueglein, Pearce, Rosso, Appel and Kappler, 2015; Sundman, Byrne, Bauer, Menguy and Kappler, 2017; Bayer, Wei, Kappler and Byrne, 2023). Additionally, about 1 mM Fe(III) was introduced due to inoculation of culture KS, which was pre-cultivated on Fe(II). Due to the additional Fe(III) introduced to the system, the average Fe(II)/Fe(III)<sub>total</sub> ratio determined by ferrozine is expected to have been  $0.026 \pm 0.002$  lower, as calculated for the initial six replicates in Schott bottles.

At the end of the first oxidation period (10 days), the Fe(II)/Fe(III)<sub>total</sub> decreased to  $0.285 \pm 0.014$  in biological replicates and remained at  $0.436 \pm 0.003$  in controls, demonstrating that culture KS successfully oxidized MNPs. After washing the MNPs and less than 24 hours after adding *G. sulfurreducens*, the Fe(II)/Fe(III)<sub>total</sub> quickly increased to  $0.448 \pm 0.023$ . At the same time, the controls showed a slight decrease to  $0.402 \pm 0.003$ , presumably caused by the washing process. During the following eight days, the Fe(II)/Fe(III)<sub>total</sub> of the MNPs increased to  $0.754 \pm 0.023$ , while it slightly decreased for abiotic controls to  $0.384 \pm 0.006$ . This suggested that *G. sulfurreducens* successfully reduced the MNPs after the previous oxidation by culture KS.

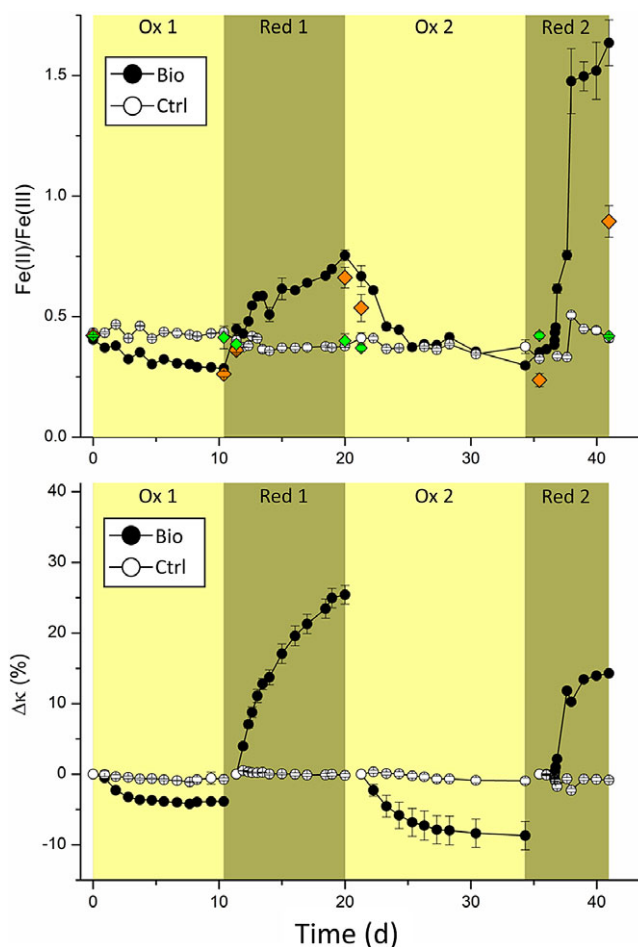


**Figure 1.** (a) Changes in the Fe(II)/Fe(III) ratio determined by ferrozine assay over time and (b) relative changes of magnetic susceptibility ( $\Delta\kappa$  in %), with respect to the starting value of each oxidation or reduction cycle, of MNPs incubated with either culture KS (yellow background) or *G. sulfurreducens* (green background). Symbols and error bars represent the mean and standard deviation of at least five replicates for Fe ratio and six replicates for  $\Delta\kappa$ . Controls were performed in triplicate. Black circles show biological replicates and white circles show controls.

As expected, the trend in relative magnetic susceptibility changes  $\Delta\kappa$  closely followed the changes observed in the Fe(II)/Fe(III)<sub>total</sub>. After the first oxidation,  $\Delta\kappa$  was  $-3.86 \pm 0.19\%$  for the experimental replicates and only  $-0.74 \pm 0.21\%$  for the controls (Fig. 1b). Possible partial dissolution of the MNPs in the growth medium is a reasonable explanation. For the first reduction,  $\Delta\kappa$  greatly increased to  $+25.42 \pm 1.31\%$  and did not change for controls at  $-0.18 \pm 0.25\%$ . Previous investigations with *G. sulfurreducens* in cell suspension experiments with magnetite showed only relative increases of  $\Delta\kappa$ , between 12% (Byrne et al., 2016) and 16.5% (Byrne, Klueglein, Pearce, Rosso, Appel and Kappler, 2015), whereas we showed a much greater increase. This demonstrated that the reduction of MNPs can happen over extended time frames and to even greater extents than previously demonstrated. While the dissolution of MNPs by *G. sulfurreducens* was previously reported and correlated with increased concentrations of dissolved  $\text{Fe}^{2+}$  (Byrne, Klueglein, Pearce, Rosso, Appel and Kappler, 2015), we could not detect any aqueous Fe. Presumably, the reduction rate plays an essential role in the fate of Fe(II)/ $\text{Fe}^{2+}$  produced during the reduction of MNPs by *G. sulfurreducens*. A lower inoculum concentration (that is, fewer initial bacteria) could have resulted in lower reduction rates of MNPs, giving the produced  $\text{Fe}^{2+}$  enough time

to interact with the surface of MNPs and, therefore, not remain as dissolved  $\text{Fe}^{2+}$ .

Notably, during the change from first reduction to second oxidation, one of the experimental replicates was compromised, and the following geochemistry data were calculated with averages and standard deviations of five instead of the previous six replicates.

During the second oxidation, the  $\text{Fe(II)/Fe(III)}_{\text{total}}$  decreased over 13 days to  $0.297 \pm 0.014$ . Due to an initially high ratio of 0.754, we could determine a much greater change during the second oxidation compared to the first, where the  $\text{Fe(II)/Fe(III)}_{\text{total}}$  decreased from 0.404 to 0.285 ( $-0.119$ ). The relative change of the  $\text{Fe(II)/Fe(III)}_{\text{total}}$  during the second oxidation, with a decrease of  $-0.457$  from 0.754 to 0.297, was almost four times greater than that of the first oxidation. However, the final  $\text{Fe(II)/Fe(III)}_{\text{total}}$  at the end of both oxidations did not greatly differ ( $0.285 \pm 0.014$  after the first and  $0.297 \pm 0.014$  after the second oxidation). This suggests that culture KS oxidized all available Fe(II) of MNPs during both oxidations. Interestingly, this suggests that MNPs charged with electrons by *G. sulfurreducens* were a much more accessible and electron-rich source. During the first 28 hours of the second reduction, the  $\text{Fe(II)/Fe(III)}_{\text{total}}$  increased from  $0.297 \pm 0.014$  to  $0.383 \pm 0.012$ . Only six hours later the  $\text{Fe(II)/Fe(III)}_{\text{total}}$  was  $0.616 \pm 0.019$ . Interestingly, the  $\text{Fe(II)/Fe(III)}_{\text{total}}$  continuously increased to a value of  $1.64 \pm 0.10$  at the end of the experiment. This extremely high ratio suggests other processes than the reduction of MNPs occurred. For controls, the  $\text{Fe(II)/Fe(III)}_{\text{total}}$  remained at  $0.41 \pm 0.02$ , a relative decrease of roughly 5% compared to  $t = 0$ .

Magnetic susceptibility measurements showed a relative decrease for the second oxidation of  $-8.70 \pm 1.99\%$  for experimental replicates, compared to just  $-0.94 \pm 0.41\%$  for controls. A two-times greater  $\Delta\kappa$  was achieved during the second oxidation than the first. These results agreed with the findings of ferrozine measurements and again showed that the electrons in the charged MNPs were a better electron source for KS than unaltered MNPs. While the  $\text{Fe(II)/Fe(III)}_{\text{total}}$  immediately changed during the second reduction,  $\Delta\kappa$  initially showed negligible changes, increasing by  $1 \pm 0.18\%$  after 31 hours. At this time point, the  $\text{Fe(II)/Fe(III)}_{\text{total}}$  ratio had already reached a value of  $0.46 \pm 0.01$ . After that, the magnetic susceptibility increased rapidly to  $+11.8 \pm 0.40\%$  in just 20 hours and eventually plateaued at  $+14\%$ , which was comparatively low regarding the  $\Delta\kappa$  of  $+25\%$  during the first reduction. The general trends of the  $\Delta\kappa$  results differed from the  $\text{Fe(II)/Fe(III)}_{\text{total}}$  results. However, it is essential to remember that magnetic susceptibility only measured the magnetic components whereas the  $\text{Fe(II)/Fe(III)}_{\text{total}}$  ratios by ferrozine incorporated all magnetic and non-magnetic components. Hence, magnetic susceptibility values that exclusively report changes to the MNPs suggest that the capacity of MNPs to be reduced by *G. sulfurreducens* could have been inhibited during the second reduction. An inhibition of reduction could have been caused by surface passivation of MNPs due to microbially derived organic compounds, which have been shown to interact with the surfaces of iron oxides (Eusterhues, Wagner, Häusler, Hanzlik, Knicker, Totsche, Kögel-Knabner and Schwertmann, 2008). However, since we saw a concomitant increase of Fe(II) with ferrozine, another Fe(II) containing phase must have been produced, which increased the Fe(II) but not  $\kappa$ . Additionally, while most of the discussed changes in the measured  $\text{Fe(II)/Fe(III)}_{\text{total}}$  and  $\Delta\kappa$  were arguably caused by redox changes in MNPs, the high increase of the  $\text{Fe(II)/Fe(III)}_{\text{total}}$  ratio during the second reduction to 1.64 seemed unrealistic. To explain this, Fe(II) or  $\text{Fe}^{2+}$  produced during reductions must have ended in different sinks. Additionally, the  $\Delta\kappa$  only increased to  $+14\%$  during the second reduction compared to  $+26\%$  during the first. As the relative change in magnetic susceptibility is linked to a change in the MNPs,

these results also suggest the presence of an additional process, and we assume that a partial dissolution of MNPs happened during the long-term incubation with *G. sulfurreducens*. Since no aqueous Fe phase was detected throughout the experiment, the comparatively slow reduction with 10% inoculum of *G. sulfurreducens* allowed  $\text{Fe}^{2+}$  to associate with MNPs or possibly reprecipitate with available phosphate and carbonate, which are both present in the microbial growth medium. While the  $\text{Fe(II)/Fe(III)}_{\text{total}}$  would have suggested a continuous reduction of magnetite, the magnetic susceptibility revealed that the reduction must have led to this reductive dissolution of the mineral (Cornell and Schwertmann, 2003) to increase Fe(II) concentration without increasing magnetic susceptibility. As determined by  $\mu$ -XRD, the Fe(II) phosphate vivianite ( $\text{Fe}^{\text{II}}_3(\text{PO}_4)_2 \cdot 8\text{H}_2\text{O}$ ) precipitated. As it has a comparatively low magnetic susceptibility with a peak value of  $5.24 \times 10^{-6} \text{ m}^3\text{kg}^{-1}$  at 37 K (Frederichs, von Dobeneck, Bleil and Dekkers, 2003), which is approximately 300 times smaller than the magnetite magnetic susceptibility of  $5.2 \times 10^{-4} \text{ m}^3\text{kg}^{-1}$  (Heider, Zit-zelsberger and Fabian, 1996), it did not interfere with the measurements of  $\kappa$ . Controls of magnetic susceptibility measurements showed no greater change than  $-1 \pm 0.43\%$  throughout the experiment.

### Mössbauer spectroscopy

Samples for  $^{57}\text{Fe}$  Mössbauer spectroscopy were taken at the start of the experiment and the end of each oxidation/reduction to further investigate the mineral identities and better understand the fate of MNPs. After inoculating with culture KS, the Mössbauer spectrum (Fig. 2a) showed two characteristic sextets that corresponded to the Fe in octahedral (grey) and tetrahedral (light blue) coordination. At 140 K, the two sextets showed some distinct features on the left-hand side while overlapping on the right-hand side, as commonly observed with nanoparticulate magnetite (Gorski and Scherer, 2010). The spectral areas of octahedral and tetrahedral Fe were used to calculate the  $\text{Fe(II)/Fe(III)}_{\text{mag}}$  ratio in the magnetite (Gorski and Scherer, 2010). The  $\text{Fe(II)/Fe(III)}_{\text{mag}}$  after the addition of culture KS was calculated as  $0.44 \pm 0.01$ . Fitting required the incorporation of an additional doublet with a small isomer shift and quadrupole splitting, which was identified as a Fe(III) phase (Fig. 2a, light green). Since no Fe(III) was detected before inoculation, the doublet was exclusively caused by inoculation with the Fe(II)-oxidizing culture KS. As washing the cells before inoculation resulted in no MNP-oxidation in test experiments, this Fe(III) phase of approximately 1 mM concentration was unavoidable. We calculated the  $\text{Fe(II)/Fe(III)}_{\text{mag}}$  after the first oxidation (Fig. 2b) as  $0.39 \pm 0.02$  (Tables S1–2), showing that MNP oxidation correlated with the change in magnetic susceptibility of  $-3.86 \pm 0.19\%$ , and showed a greater ratio than ferrozine ( $0.285 \pm 0.014$ ). The Mössbauer fit after the first oxidation again required a Fe(III) doublet (Fig. 2b, light green) corresponding to the Fe(III) added with the inoculum.

At the end of the first reduction (Fig. 2c), the two sextets remained, showing the integrity of the MNPs even after reduction. No more Fe(III) was detected, suggesting that if any Fe(III) remained despite the washing, the readily available poorly crystalline ferrihydrite, which is the oxidation product of culture KS (Nordhoff, Tominski, Halama, Byrne, Obst, Kleindienst, Behrens and Kappler, 2017; Bayer, Tomaszewski, Bryce, Kappler and Byrne, 2023), was reduced by *G. sulfurreducens*. The fit required a doublet with a large isomer shift and quadrupole splitting (Fig. 2c, red), indicative of a newly formed Fe(II) phase. This Fe(II) phase was much more abundant than the previously detected Fe(III), with a relative area of  $17.92 \pm 0.51\%$ . Even if the washing step did not remove any Fe(III) after oxidation, it could still not explain such

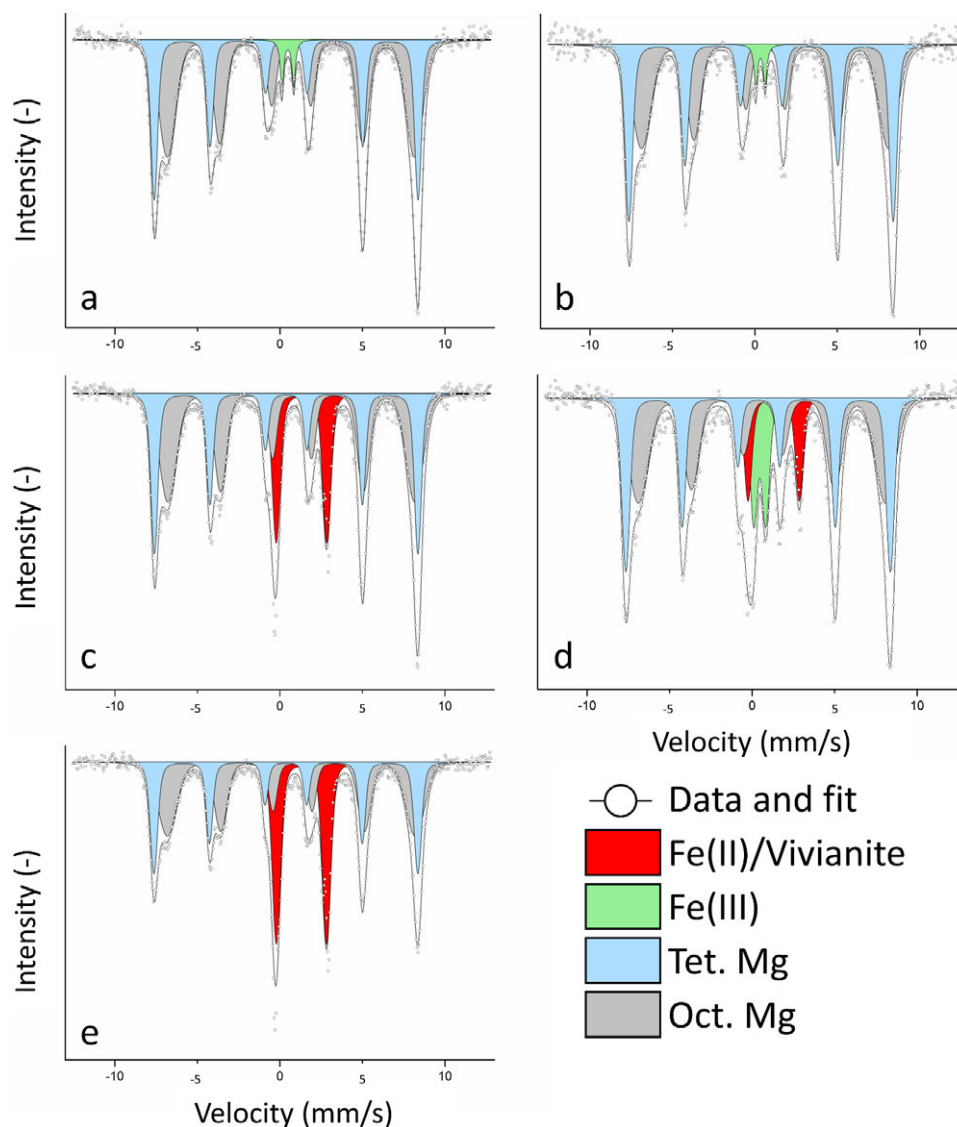


**Figure 2.**  $^{57}\text{Fe}$  Mössbauer spectra of MNPs collected at 140 K at (a) the start and (b) the end of the first oxidation, (c) after the first reduction, (d) after the second oxidation, and (e) after the second reduction. Characteristic sextets of tetrahedral (light blue) and octahedral (grey) magnetite could be observed. We additionally detected a Fe(III) phase (light green) due to inoculation with culture KS and a Fe(II) phase (red), which was confirmed to be (partially) vivianite.

a large Fe(II) doublet. Comparing the obtained isomer shift and quadrupole splitting values (Table S2), one of the closest matches was the Fe(II) phosphate vivianite (Wilfert, Dugulan, Goubitz, Korving, Witkamp and Van Loosdrecht, 2018), a reasonable assumption for our system (Miot, Benzerara, Morin, Bernard, Beyssac, Larquet, Kappler and Guyot, 2009). The calculated  $\text{Fe(II)/Fe(III)}_{\text{mag}}$  was  $0.42 \pm 0.01$ . While this ratio was much smaller than the determined ratio with ferrozine ( $0.75 \pm 0.023$ ), we could now show that the high ferrozine values were biased by newly formed Fe(II) phases, and we propose that the actual value was closer to the one determined by Mössbauer spectroscopy. Additionally, since  $\Delta\kappa$  continuously increased, we assume that the reduction of magnetite and dissolution-reprecipitation happened simultaneously as the formation of vivianite could not have explained the changes in  $\Delta\kappa$  values.

After the second oxidation, we detected four different phases (Fig. 2d): the two MNP sextets (light blue, grey), Fe(II) (red) and Fe(III) (light green). The Fe(III) doublet had a much greater spectral area ( $11.26 \pm 0.66\%$ ) than the first oxidation ( $2.83\%$ ). A higher spectral area of roughly 4% for Fe(III), due to the inoculum of culture KS, was not expected. The high value for Fe(III)

indicated that previously formed Fe(II) was not successfully removed by washing and magnetic separation. We suggest that some of the transferred Fe(II) was vivianite that culture KS was unable to oxidize, as previously reported (Tominski, Heyer, Lösekann-Behrens, Behrens and Kappler, 2018; Bayer, Tomaszewski, Bryce, Kappler and Byrne, 2023), while other transferred Fe(II) phases were used as electron sources, resulting in a larger Fe(III) spectral area. Remembering the data shown in Fig. 1, we assume that this oxidation of a non-magnetic bioavailable Fe(II) phase happened towards the end of the second oxidation since  $\Delta\kappa$  (Fig. 1b) did not decrease anymore, but the  $\text{Fe(II)/Fe(III)}_{\text{total}}$  ratio did (Fig. 1a). We concluded that reduced MNPs were a preferred electron donor for culture KS even in the presence of other Fe(II) phases. This could be attributed to a more negative redox potential of highly-reduced MNPs, again suggesting that the additional Fe(II) phase was oxidized after MNP oxidation became less favourable (Gorski, Nurmi, Tratnyek, Hofstetter and Scherer, 2010; Dong, Zeng, Sheng, Chen, Yu and Kappler, 2023). The remaining Fe(II) at the end of the second oxidation should have consisted of vivianite. The calculated ratio of the MNPs after the second oxidation was  $0.40 \pm 0.02$ .



Finally, after the last reduction, we could determine the two sextets (MNPS) and one Fe(II) doublet (Fig. 2e), which now corresponded to one-third of the spectral area ( $29.94 \pm 0.60\%$ ). We again assume that most of this Fe(II) phase was vivianite. However, other Fe(II) phases such as siderite ( $\text{FeCO}_3$ , due to the presence of bicarbonate buffer) were likely, since the isomer shift and quadrupole splitting were not conclusive for either vivianite or siderite (Table S2). This large increase in Fe(II) explains the great increase in the Fe(II)/Fe(III)<sub>total</sub> ratio as determined by ferrozine (Fig. 1a). During MNPs reduction, dissolved aqueous  $\text{Fe}^{2+}$  could have either interacted with magnetite particles or precipitated as a Fe(II) contributing to the doublet that was determined with Mössbauer spectroscopy. Since  $\Delta\kappa$  changed much less during the second reduction, we assume that the MNP-dissolution was now more pronounced and that continuous cycling led to an overall loss of minerals, questioning the biogeobattery capacities of MNPs over many consecutive redox cycles. After the second reduction, the Fe(II)/Fe(III)<sub>mag</sub> was  $0.42 \pm 0.01$ . A control was measured at the end of the second reduction, which showed minor changes compared to the control at  $t = 0$  (Fig. S3). The changes in spectral areas are displayed in Fig. S3.

During the first reduction, the trends in ferrozine Fe(II)/Fe(III)<sub>total</sub> ratios,  $\Delta\kappa$  (Fig. 1) and the calculated Mössbauer Fe(II)/Fe(III)<sub>mag</sub> ratios (Table S2) suggested that the reduction of MNPs could have proceeded for a longer time. Previously, ratios of up to 0.46 after reduction, determined by Mössbauer at 140 K, were described (Byrne, Klueglein, Pearce, Rosso, Appel and Kappler, 2015). The greater the Fe(II)/Fe(III) ratios we present here, and the previous absence of any Fe(II) doublets in Mössbauer spectra, imply that the rate and duration of reduction greatly influenced the fate of MNPs. Previously, it was shown that the rate of Fe(II) reduction had consequences for the formation of secondary minerals (Dippon, Schmidt, Behrens and Kappler, 2015) and that the reduction rate of ferrihydrite influenced the formation of magnetite or other Fe minerals (Han, Tomaszewski, Sorwat, Pan, Kappler and Byrne, 2020). We expand on this knowledge by proposing that, in an MNP-biogeobattery system, the rate of Fe(II) oxidation and especially Fe(III) reduction is of great importance for the fate of  $\text{Fe}^{2+}/\text{Fe}$  (II). While no newly formed Fe(II) phases could be detected in comparatively short experiments with high cell densities (Byrne, Klueglein, Pearce, Rosso, Appel and Kappler, 2015), we showed that low inoculum and an extended timeframe for oxidation/reduction promoted reductive dissolution and reprecipitation. We conclude that the incubation of MNPs as a biogeobattery will eventually lead to the reductive dissolution of the mineral. This dissolution will be more pronounced with an increasing number of redox cycles.

### X-ray diffractometry (XRD)

Samples for  $\mu\text{XRD}$  were collected at the start of the experiment and after every oxidation and reduction phase for biotic samples and controls (Fig. 3). For the initial phases, only reflections that can be assigned to magnetite were detected, with three main reflections at  $2\theta$  of:  $43.36^\circ$ ,  $50.50^\circ$  and  $35.11^\circ$ . Only magnetite was identified, since the ferrihydrite added with culture KS (see the previous discussion) typically does not yield a clear diffraction pattern with the Co-source used for X-ray generation (CoK $\alpha$  radiation,  $\lambda = 0.17903$  nm). This did not change after the first oxidation.

After the first reduction, we could see the same main reflections caused by magnetite. Additionally, the signal seemed generally noisier between  $2\theta$  of  $30^\circ$  to  $50^\circ$ , which we could not identify as a specific mineral phase. Two minor reflections could be seen at  $2\theta$  of  $15^\circ$  and  $38^\circ$ , which corresponded with the main reflections and an

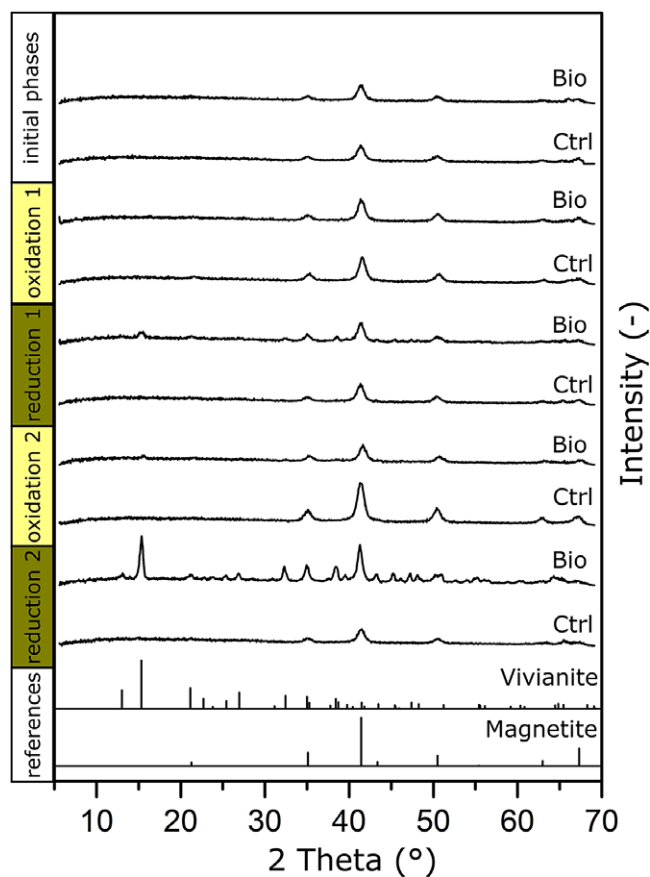


**Figure 3.**  $\mu\text{XRD}$  patterns of MNPs collected before the experiment (initial phases) and at the end of each oxidation/reduction for the biotic experiments (Bio) and the abiotic controls (Ctrl). References of vivianite and magnetite are shown at the bottom.

additional reflection of vivianite:  $\mu\text{XRD}$  confirmed that vivianite had already formed during the first reduction.

For the second oxidation, both the sample and the control showed only the three main reflections of magnetite at  $2\theta$  of  $43.36^\circ$ ,  $50.50^\circ$  and  $35.11^\circ$ , with some minor reflection remaining at  $2\theta$  of  $15.32^\circ$  (vivianite). This agreed with the Mössbauer measurement, which showed that a Fe(II) phase remained even after the second oxidation. As previously discussed, this Fe(II) phase initially consisted of vivianite and possibly other Fe(II) phases (for example, siderite). While culture KS could have used additional Fe(II) phases as electron sources, vivianite remained because culture KS could not use it as an electron source (Tominski, Heyer, Lösekann-Behrens, Behrens and Kappler, 2018).

After the second reduction, the most intense reflection ( $2\theta$   $15.32^\circ$ ) corresponded to the main reflection of vivianite, and further reflections of vivianite were observed (Fig. 3). We could again confirm vivianite as a product during long-term low-volume incubations of MNPs as a biogeobattery in our system.

We additionally compared matches with the reflections of siderite ( $\text{FeCO}_3$ ) as it could have precipitated in  $\text{HCO}_3^-$ -containing medium. We could show that the first and fourth main reflections ( $2\theta$   $32.17^\circ$  and  $38.45^\circ$ ) closely matched our diffraction pattern (Fig. S4, black dotted lines). However, since only two of the six most intense reflections of siderite could be seen (Fig. S4, grey dotted lines), we cannot confirm its presence with certainty. We again suggest that more than one Fe(II) phase was present in our system, that the main phase was the Fe(II) phosphate vivianite and

that the remainder could have been siderite and other Fe(II)-containing phases.

We calculated the lattice parameters and average crystal diameter ( $d_{\mu\text{XRD}}$  in nm) from collected  $\mu\text{-XRD}$  patterns (Table S1). The synthesized MNPs had a size of 10.07 nm and a sample inoculated with culture KS 9.97 nm. The diameter of the abiotic controls showed little change throughout the experiment ( $d_{\text{XRD}} = 10.2120 \text{ nm} \pm 0.0006 \text{ nm}$ ). The diameters of the biotic samples changed as follows (start ox 1, end ox 1, end red 1, end ox 2, end red 2): 10.07 nm, 9.18 nm, 12.31 nm, 10.88 nm, 17.76 nm. The calculated diameter after reductions (12.31 nm and 17.76 nm) increased by 22% and 76% compared to the initial value. Since we confirmed the presence of vivianite, which has overlapping reflections with magnetite at  $2\theta$  of  $41.4^\circ$ , it likely influenced the lattice parameters and average crystal diameter calculation. With increasingly more vivianite present, the calculated crystal size was decreasingly representative of the MNPs.

### Infrared spectroscopy

FTIR spectra were collected from two biotic samples and one control after the second oxidation and from three biotic samples and one control after the second reduction (Fig. 4). All samples showed characteristic vibrations of Fe-O bonds at approximately  $565 \text{ cm}^{-1}$ , which were mainly caused by the added MNPs. The peaks widened for the samples collected after the second reduction (Fig. 4c-e), which indicates that additional Fe-O bonds were present in the system (Skulte, Kashyap, Dyar, Holden, Tague, Wang and Jaret, 2018). Since vivianite was abundant, especially after the second reduction, we could see four vibration bands of approx.  $819, 939, 975$  and  $1051 \text{ cm}^{-1}$  corresponding to P-O bonds (Frost, Martens, Williams and Klopogge, 2002), which only had muted intensities after oxidations and in controls (Fig. 4). Additional vibrations at higher wave numbers of approx.  $1620 \text{ cm}^{-1}$ ,  $3140 \text{ cm}^{-1}$  and  $3500 \text{ cm}^{-1}$  were caused by O-H vibrations, which were present in all samples. The increased signals of Fe-O and P-O

bonds, especially after the reductions, confirmed the formation of vivianite as a result of Fe reduction and reprecipitation.

### Scanning electron microscopy

After the second reduction, samples were prepared for FE-SEM analysis (Fig. 5). Micrographs indicated that MNPs had a diameter of roughly 10 to 12 nm (Fig. 5a), which agrees with the initial XRD calculated diameter ( $d_{\text{XRD}} = 10.07$  for biotic samples and 10.21 nm for controls), which could underline the influence of abundant vivianite on the diameter determination with  $\mu\text{XRD}$  after reductions. Vivianite was also observed (Fig. 5b, d-f), agreeing with results from  $\mu\text{XRD}$  and  $^{57}\text{Fe}$  Mössbauer spectroscopy.

Almost intact cells and cell fragments of *G. sulfurreducens* were observed (Fig. 5c-d), as indicated by blue arrows in the respective micrographs. As the samples were not fixed with glutaraldehyde, the cellular structure was not preserved throughout sample preparation and analysis. MNPs appeared to cover the surface of the vivianite crystals, in close contact and sometimes nested within vivianite surface defects (Figs 5b and 5d-f, blue arrows). While sample preparation is essential for SEM analysis, we propose that this close interaction of vivianite and magnetite was not solely a preparation artefact. We hypothesize that the close interactions of vivianite and MNPs caused carry-over of Fe(II)-phases between reduction and oxidation redox half-cycles, despite washings. Additional micrographs are displayed in Fig S5.

### Conclusions

We investigated the viability of magnetite nanoparticles (MNPs) to serve as biogeochemical batteries in two consecutive redox cycles with growing bacteria and followed changes in biogeochemistry and mineralogy over time. Our results showed that MNPs were successfully used as an electron source and sink over 41 days by the autotrophic nitrate-reducing Fe(II)-oxidizing culture KS and the Fe(III)-reducing *Geobacter sulfurreducens*. Changes in magnetic susceptibility and

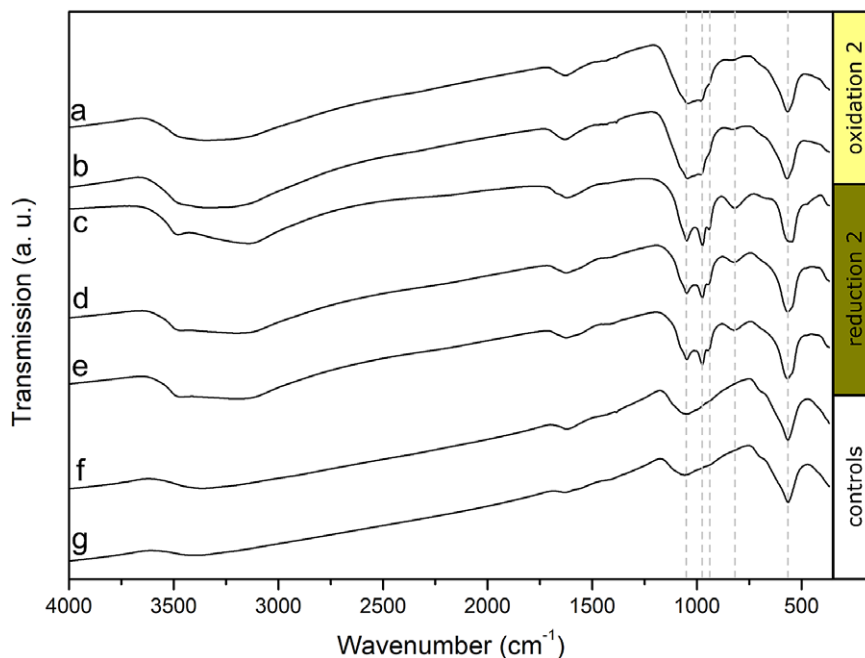


**Figure 4.** Fourier-transformed infrared (FTIR) spectra of anoxically dried magnetite samples. (a-b) Biological replicates collected after the second oxidation, (c-e) biological replicates collected after the second reduction, (f) control collected after the second oxidation, (g) control collected after the second reduction.



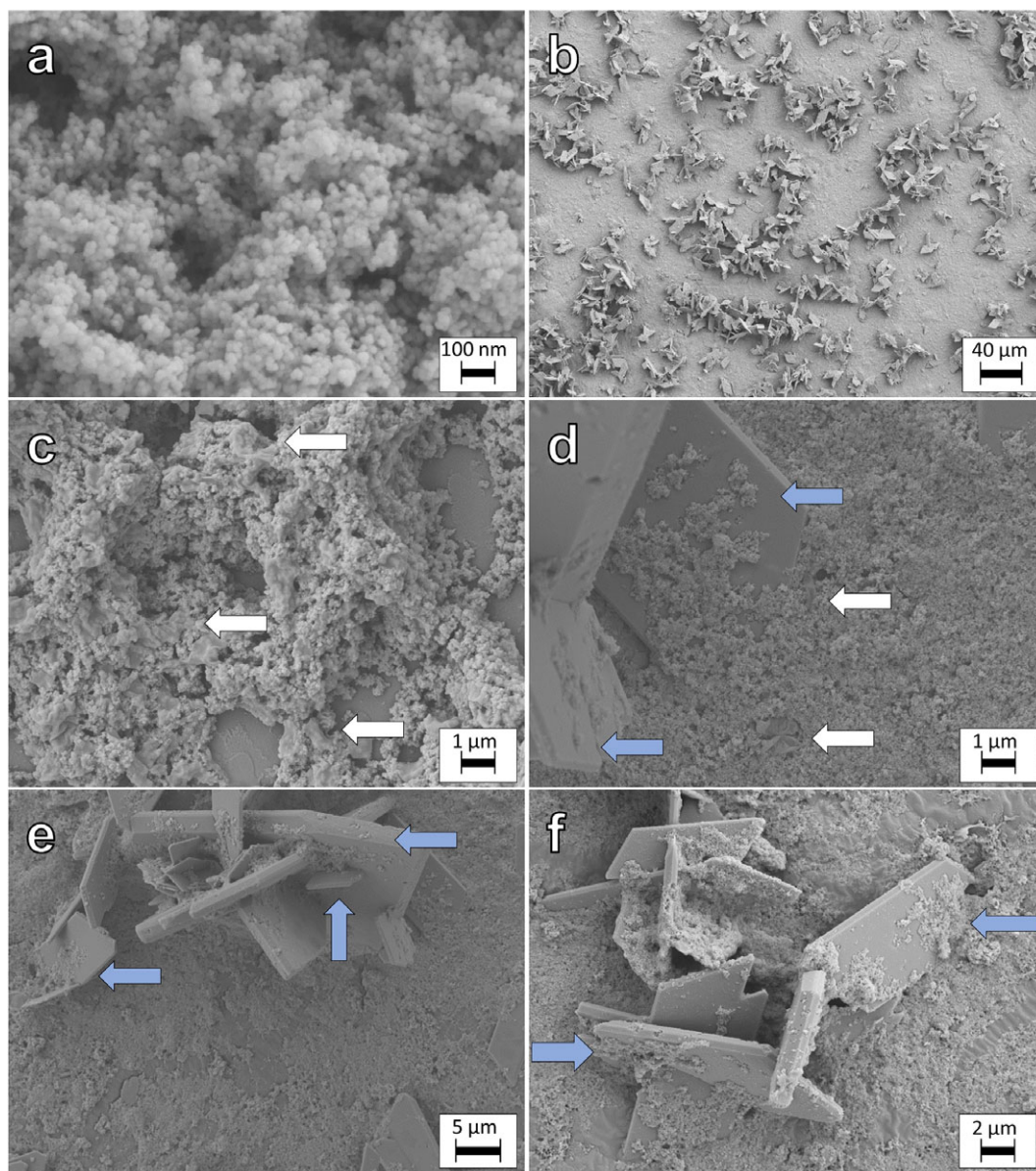


**Figure 5.** SEM images of samples collected at the end of the second reduction. (a) High magnification of MNPs, (b) overview of MNPs and newly formed vivianite, (c) remains of biomass/cells (presumably *G. sulfurreducens*) (cells were not fixed with glutaraldehyde), (d) close contact of MNPs and formed vivianite and cells, (e-f) characteristic twinning of vivianite crystals and close contact with MNPs. White arrows point to cells and blue arrows to MNPs-vivianite associations.

Fe(II)/Fe(III) ratio showed successful oxidation of MNPs by culture KS, as previously described (Bayer, Wei, Kappler and Byrne, 2023). The second oxidation resulted in a greater decrease in relative magnetic susceptibility  $\Delta\kappa$  than the first (−8.7% vs. −3.9%). This demonstrated that the ‘charged’ MNPs, due to reduction by *G. sulfurreducens*, were a favourable electron source for culture KS. These findings were supported by the change of the Fe(II)/Fe(III)<sub>total</sub> ratio, which decreased by −0.119 for the first and by −0.457 for the second oxidation. The lowest measured Fe(II)/Fe(III)<sub>total</sub> ratio detected during the entire experiment was 0.24, a point where the increasingly positive redox potential of ‘discharged’ MNPs potentially does not allow further oxidation. During the reduction of MNPs by *G. sulfurreducens*, secondary Fe(II) minerals formed, as

determined by Mössbauer spectroscopy,  $\mu$ XRD and SEM. Even in the presence of these Fe(II) phases, culture KS prioritized oxidation of MNPs as we showed by comparing changes in Fe(II)/Fe(III)<sub>total</sub> to  $\Delta\kappa$ . Interestingly, the changes in  $\Delta\kappa$  were smaller for the second reduction than for the first (+14.3% vs. +25.42%). This suggests that the capacity for MNPs to serve as an electron sink might diminish over time due dissolution of MNPs or further processes like passivation (Byrne *et al.*, 2016). Due to clear evidence of increased vivianite precipitation, we suggest that the second reduction resulted in a more pronounced reductive dissolution followed by reprecipitation. We also suggest that the extent of reductive dissolution and reprecipitation will be increasingly pronounced with every additional redox cycle. The identity of vivianite was confirmed by  $\mu$ XRD and SEM.

Additional Fe(II) phases were detected but could not be identified conclusively, likely due to the poor crystallinity of these minerals, although some  $\mu$ XRD reflections point towards siderite formation. The demonstrated dissolution and reprecipitation of  $\text{Fe}^{2+}$  suggested that the  $\text{Fe(II)/Fe(III)}_{\text{total}}$  ratio determined by the ferrozine assay was influenced by these newly formed Fe(II) phases and that the  $\text{Fe(II)/Fe(III)}_{\text{mag}}$  ratio in MNPs – especially during reductions – was indeed lower than measured by the ferrozine assay.

While we demonstrated the biogeobattery functioning of MNPs in consecutive redox cycles, prolonged redox cycling did not only greatly influence the  $\text{Fe(II)/Fe(III)}$  ratio as expected, but resulted in mineral dissolution that represents a loss of MNPs over time. We suggest that, without additional processes that would form MNPs in the environment, such as Fe oxidation and reduction, MNPs will be consumed over time. While Fe(II)-oxidizers would greatly benefit from reduced (electron-rich) MNPs, the Fe(III)-reducers would eventually have to rely on a different electron sink. However, the newly formed Fe(II) phases could also result in losing a usable electron source for Fe(II)-oxidizers, as we show in our experiments with culture KS and the inability to oxidize newly formed vivianite. We suggest that an MNP biogeobattery can support the redox cycling of Fe-metabolizing bacteria; however, this will disappear over time if no further processes result in the formation of MNPs, which were unlikely in our system. Finally, we show the great importance of contact time between bacteria and Fe-minerals and suggest that the results might be different according to the length of redox cycles, where short-term redox cycles can, presumably, maintain the integrity of the MNPs contrary to the here presented results of long-term incubations. The presented results have significant implications for the (bio)availability of contaminants and nutrients associated with the surface of MNPs. Over time, the remediation capacities of MNPs will decrease during continued redox cycling due to dissolution. The stability of MNPs and the formation and transformation of secondary minerals will determine the fate of contaminants and nutrients and the long-term activity of Fe-metabolizing bacteria.

**Supplementary material.** The supplementary material for this article can be found at <https://doi.org/10.1180/gbi.2024.2>.

**Author contribution.** Timm Bayer and James Byrne conceived the research. Timm Bayer performed experiments and most analytical measurements. Natalia Jakus performed  $\mu$ XRD measurements. James Byrne and Andreas Kappler supervised the research. The research was funded by financial support granted to James Byrne and Andreas Kappler. The manuscript was written through the contributions of all authors, and all authors have given their approval to the final version of the manuscript.

**Acknowledgements.** The authors thank the editors and two random reviewers for handling and improving the quality of the manuscript with helpful comments. This work was financed through funding awarded to James Byrne (BY 82/2-1) and Andreas Kappler (KA 1736/48-1). The authors thank Lars Grimm for freeze drying and BET analysis, Biao Wan for FTIR measurements, Franziska Schädler for FIA measurements, Verena Nikeleit for HPLC measurements and Jeremiah Schuster and Stefan Fischer for help with and access to the electron microscope. We gratefully acknowledge the Tübingen Structural Microscopy Core Facility, funded by the Excellence Strategy of the German Federal and State Governments, for their support and assistance in this work. James Byrne is supported by a UKRI Future Leaders Fellowship (MR/V023918/1). Andreas Kappler acknowledges infrastructural support by the Deutsche Forschungsgemeinschaft (DFG, German Research Foundation) under Germany's Excellence Strategy, Cluster of Excellence EXC2124, project ID 390838134.

**Competing interest.** The authors declare no competing financial interest.

## References

- Amor, M., Tharaud, M., Gélabert, A. and Komeili, A. (2020) Single-cell determination of iron content in magnetotactic bacteria: Implications for the iron biogeochemical cycle. *Env. Microbiol.*, **22**, 823–31. <https://doi.org/10.1111/1462-2920.14708>
- Bayer T., Tomaszewski, E.J., Bryce, C., Kappler, A. and Byrne, J.M. (2023) Continuous cultivation of the lithoautotrophic nitrate-reducing Fe(II)-oxidizing cultures in a chemostat bioreactor. *Env. Microbiol. Rep.*, **15**(4), 324–334. <https://doi.org/10.1111/1758-2229.13149>
- Bayer, T., Wei, R., Kappler, A. and Byrne, J.M. (2023) Cu(II) and Cd(II) removal efficiency of microbially redox-activated magnetite nanoparticles. *ACS Earth Space Chem.* **7** (10), 1837–1847. <https://doi.org/10.1021/acsearthspacechem.2c00394>
- Bryce, C., Blackwell, N., Schmidt, C., Otte, J., Huang, Y.M., Kleindienst, S., Tomaszewski, E., Schad, M., Warter, V. and Peng, C. (2018) Microbial anaerobic Fe(II) oxidation—ecology, mechanisms and environmental implications. *Env. Microbiol.*, **20**, 3462–83. <https://doi.org/10.1111/1462-2920.14328>
- Byrne, J.M. and Amor, M. (2023) Biomagnetism: Insights into magnetic minerals produced by microorganisms. *Elements*, **19**, 208–14. <https://doi.org/10.2138/gselements.19.4.208>
- Byrne, J.M., Klueglein, N., Pearce, C., Rosso, K.M., Appel, E. and Kappler, A. (2015) Redox cycling of Fe(II) and Fe(III) in magnetite by Fe-metabolizing bacteria. *Sci.*, **347**, 1473–76. <https://doi.org/10.1126/science.aaa4834>
- Byrne, J.M., van der Laan, G., Figueroa, A.I., Qafoku, O., Wang, C., Pearce, C.I., Jackson, M., Feinberg, J., Rosso, K.M. and Kappler, A. (2016) Size dependent microbial oxidation and reduction of magnetite nano- and micro-particles. *Sci. Rep.*, **6**, 30969. <https://doi.org/10.1038/srep30969>
- Cornell, R.M. and Schwertmann, U. (2003) *The iron oxides: Structure, properties, reactions, occurrences and uses* (2nd ed.). Wiley-VCH, Weinheim, Germany. <https://doi.org/10.1002/3527602097>
- Dippon, U., Schmidt, C., Behrens, S. and Kappler, A. (2015) Secondary mineral formation during ferrihydrite reduction by *Shewanella oneidensis* Mr-1 depends on incubation vessel orientation and resulting gradients of cells,  $\text{Fe}^{2+}$  and Fe minerals. *Geomicrobiol. J.*, **32**, 878–89. <https://doi.org/10.1080/01490451.2015.1017623>
- Dong, H., Zeng, Q., Sheng, Y., Chen, C., Yu, G. and Kappler, A. (2023) Coupled iron cycling and organic matter transformation across redox interfaces. *Nat. Rev. Earth Environ.*, **4**, 659–73. <https://doi.org/10.1038/s43017-023-00470-5>
- Dong, Y., Sanford, R.A., Boyanov, M.I., Flynn, T.M., O'Loughlin, E.J., Kemmer, K.M., George, S., Fouke, K.E., Li, S., Huang, D., Li, S. and Fouke, B.W. (2020) Controls on iron reduction and biomineralization over broad environmental conditions as suggested by the firmicutes *Oreana metallireducens* strain z6. *Environ. Sci. Technol.*, **54**, 10128–40. <https://doi.org/10.1021/acs.est.0c03853>
- Emerson, D. and Moyer, C. (1997) Isolation and characterization of novel iron-oxidizing bacteria that grow at circumneutral pH. *Appl. Environ. Microbiol.*, **63**, 4784–92. <https://doi.org/10.1128/aem.63.12.4784-4792.1997>
- Eusterhues, K., Wagner, F.E., Häusler, W., Hanzlik, M., Knicker, H., Totsche, K.U., Kögel-Knabner, I. and Schwertmann, U. (2008) Characterization of ferrihydrite-soil organic matter coprecipitates by x-ray diffraction and mossbauer spectroscopy. *Environ. Sci. Technol.*, **42**, 7891–97. <https://doi.org/10.1021/es800881w>
- Evans, M. and Heller, F. (2003) *Environmental magnetism: Principles and applications of enviromagnetics*. Elsevier, Amsterdam, Netherlands ISBN: 9780080505787.
- Frederichs, T., von Döbeneck, T., Bleil, U. and Dekkers, M.J. (2003) Towards the identification of siderite, rhodochrosite, and vivianite in sediments by their low-temperature magnetic properties. *Phys. Chem. Earth*, **28**, 669–79. [https://doi.org/10.1016/S1474-7065\(03\)00121-9](https://doi.org/10.1016/S1474-7065(03)00121-9)
- Frost, R.L., Martens, W., Williams, P.A. and Klopogge, J. (2002) Raman and infrared spectroscopic study of the vivianite-group phosphates vivianite, baricite and bobierite. *Mineralogical Magazine*, **66**, 1063–73. <https://doi.org/10.1180/0026461026660077>
- Gorski, C.A., Nurmi, J.T., Tratnyek, P.G., Hofstetter, T.B. and Scherer, M.M. (2010) Redox behavior of magnetite: Implications for contaminant reduction. *Environ. Sci. Technol.*, **44**, 55–60. <https://doi.org/10.1021/es9016848>
- Gorski, C.A. and Scherer, M.M. (2010) Determination of nanoparticulate magnetite stoichiometry by mossbauer spectroscopy, acidic dissolution, and



- powder x-ray diffraction: A critical review. *Am. Min.*, **95**, 1017–26. <https://doi.org/10.2138/am.2010.3435>
- Han, X., Tomaszewski, E.J., Sorwat, J., Pan, Y., Kappler, A. and Byrne, J.M. (2020) Effect of microbial biomass and humic acids on abiotic and biotic magnetite formation. *Environ. Sci. Technol.*, **54**, 4, 121–30. <https://doi.org/10.1021/acs.est.9b07095>
- Heider, F., Zitzelsberger, A. and Fabian, K. (1996) Magnetic susceptibility and remanent coercive force in grown magnetite crystals from 0.1  $\mu\text{m}$  to 6 mm. *Phys. Earth and Planetary Interiors*, **93**, 239–56. [https://doi.org/10.1016/0031-9201\(95\)03071-9](https://doi.org/10.1016/0031-9201(95)03071-9)
- Kappler, A., Becker, S. and Enright, A.M.L. (2021) Metals, microbes, and minerals - the biogeochemical side of life. Pp. 185–228. In K. Peter, and T. Martha Sosa, Eds. *Living on iron*, De Gruyter. <https://doi.org/10.1515/9783110589771>
- Kappler, A., Bryce, C., Mansor, M., Lueder, U., Byrne, J.M. and Swanner, E.D. (2021) An evolving view on biogeochemical cycling of iron. *Nat. Rev. Microbiol.*, **19**, 360–74. <https://doi.org/10.1038/s41579-020-00502-7>
- Kappler, A. and Straub, K.L. (2005) Geomicrobiological cycling of iron. *Rev. Min. Geochem.*, **59**, 85–108. <https://doi.org/10.2138/rmg.2005.59.5>
- Kappler, A., Thompson, A. and Mansor, M. (2023) Impact of biogenic magnetite formation and transformation on biogeochemical cycles. *Elements*, **19**, 222–227. <https://doi.org/10.2138/gselements.19.4.222>
- Kendall, B., Anbar, A.D., Kappler, A. and Konhauser, K.O. (2012) The global iron cycle. *Fundam. of Geobiol.*, **1**, 65–92. <https://doi.org/10.1002/9781118280874.ch6>
- Klueglein, N. and Kappler, A. (2013) Abiotic oxidation of Fe(II) by reactive nitrogen species in cultures of the nitrate-reducing Fe(II) oxidizer *Acidovorax* sp. Bofen1 - questioning the existence of enzymatic Fe(II) oxidation. *Geobiol.*, **11**, 180–90. <https://doi.org/10.1111/gbi.12019>
- Klug, H.P. and Alexander, L.E. (1974) *X-ray diffraction procedures: For polycrystalline and amorphous materials*. John Wiley & Sons, New York-Sydney-Toronto, **79** (6). ISBN: 978-0-471-49369-3
- Lies, D.P., Hernandez, M.E., Kappler, A., Mielke, R.E., Gralnick, J.A. and Newman, D.K. (2005) *Shewanella oneidensis* mr-1 uses overlapping pathways for iron reduction at a distance and by direct contact under conditions relevant for biofilms. *Appl. Environ. Microbiol.*, **71**, 4414–26. <https://doi.org/10.1128/AEM.71.8.4414-4426.2005>
- Liu, F., Rotaru, A.E., Shrestha, P.M., Malvankar, N.S., Nevin, K.P. and Lovley, D.R. (2015) Magnetite compensates for the lack of a pilin-associated c-type cytochrome in extracellular electron exchange. *Env. Microbiol.*, **17**, 648–55. <https://doi.org/10.1111/1462-2920.12485>
- Lovley, D.R., Stolz, J.F., Nord Jr, G.L. and Phillips, E.J. (1987) Anaerobic production of magnetite by a dissimilatory iron-reducing microorganism. *Nat.*, **330**, 252. <https://doi.org/10.1038/330252a0>
- Lovley, D.R., Ueki, T., Zhang, T., Malvankar, N.S., Shrestha, P.M., Flanagan, K.A., Aklujkar, M., Butler, J.E., Giloteaux, L. and Rotaru, A.-E. (2011) Geobacter: The microbe electric's physiology, ecology, and practical applications. *Adv. Microb. Physiol.*, **59**, 1–100. <https://doi.org/10.1016/B978-0-12-387661-4.00004-5>
- Maher, B.A. (2009) Rain and dust: Magnetic records of climate and pollution. *Elements*, **5**, 229–234. <https://doi.org/10.2113/gselements.5.4.229>
- Maher, B.A. and Taylor, R.M. (1988) Formation of ultrafine-grained magnetite in soils. *Nat.*, **336**, 368. <https://doi.org/10.1038/336368a0>
- Miot, J., Benzerara, K., Morin, G., Bernard, S., Beyssac, O., Larquet, E., Kappler, A. and Guyot, F. (2009) Transformation of vivianite by anaerobic nitrate-reducing iron-oxidizing bacteria. *Geobiol.*, **7**, 373–84. <https://doi.org/10.1111/j.1472-4669.2009.00203.x>
- Miot, J., Li, J., Benzerara, K., Sougrati, M.T., Ona-Nguema, G., Bernard, S., Jumas, J.-C. and Guyot, F. (2014) Formation of single domain magnetite by green rust oxidation promoted by microbial anaerobic nitrate-dependent iron oxidation. *Geochim. Cosmochim. Acta*, **139**, 327–43. <https://doi.org/10.1016/j.gca.2014.04.047>
- Nordhoff, M., Tominski, C., Halama, M., Byrne, J.M., Obst, M., Kleindienst, S., Behrens, S. and Kappler, A. (2017) Insights into nitrate-reducing Fe(II) oxidation mechanisms through analysis of cell-mineral associations, cell encrustation, and mineralogy in the chemolithoautotrophic enrichment culture ks. *Appl. Environ. Microbiol.*, **83**, e00752–00717. <https://doi.org/10.1128/AEM.00752-17>
- Notini, L., Byrne, J.M., Tomaszewski, E.J., Latta, D.E., Zhou, Z., Scherer, M.M. and Kappler, A. (2019) Mineral defects enhance bioavailability of goethite toward microbial Fe(III) reduction. *Environ. Sci. Technol.*, **53**, 8883–91. <https://doi.org/10.1021/acs.est.9b03208>
- Patterson, A.L. (1939) The Scherrer formula for x-ray particle size determination. *Phys. Rev.*, **56**, 978–82. <https://doi.org/10.1103/PhysRev.56.978>
- Pearce, C.I., Qafoku, O., Liu, J., Arenholz, E., Heald, S.M., Kukkadapu, R.K., Gorski, C.A., Henderson, C.M.B. and Rosso, K.M. (2012) Synthesis and properties of titanomagnetite (Fe<sub>3</sub>–xTi<sub>x</sub>) nanoparticles: A tunable solid-state Fe(II/III) redox system. *J. Colloid Interface Sci.*, **387**, 24–38. <https://doi.org/10.1016/j.jcis.2012.06.092>
- Peterson, M.L., White, A.F., Brown, G.E. and Parks, G.A. (1997) Surface passivation of magnetite by reaction with aqueous Cr(VI): Xafs and TEM results. *Environ. Sci. Technol.*, **31**, 1573–76. <https://doi.org/10.1021/es960868i>
- Porsch, K., Dippon, U., Rijal, M.L., Appel, E. and Kappler, A. (2010) In-situ magnetic susceptibility measurements as a tool to follow geomicrobiological transformation of Fe minerals. *Environ. Sci. Technol.*, **44**, 3846–52. <https://doi.org/10.1021/es903954u>
- Schüler, D. (2002) The biomineralization of magnetosomes in magnetospirillum gryphiswaldense. *International microbiology*, **5**, 209–14. <https://doi.org/10.1007/s10123-002-0086-8>
- Schaedler, F., Kappler, A. and Schmidt, C. (2017) A revised iron extraction protocol for environmental samples rich in nitrite and carbonate. *Geomicrobiol. J.*, **35**, 23–30. <https://doi.org/10.1080/01490451.2017.1303554>
- Sklute, E.C., Kashyap, S., Dyar, M.D., Holden, J.F., Tague, T., Wang, P. and Jaret, S.J. (2018) Spectral and morphological characteristics of synthetic nanophase iron (oxyhydr) oxides. *Phys. Chem. Miner.*, **45**, 1–26. <https://doi.org/10.1007/s00269-017-0897-y>
- Stookey, L.L. (1970) Ferrozine - a new spectrophotometric reagent for iron. *Anal. Chem.*, **42**, 779–81. <https://doi.org/10.1021/ac60289a016>
- Straub, K.L., Benz, M., Schink, B. and Widdel, F. (1996) Anaerobic, nitrate-dependent microbial oxidation of ferrous iron. *Appl. Environ. Microbiol.*, **62**, 1458–60. <https://doi.org/10.1128/aem.62.4.1458-1460.1996>
- Sundman, A., Byrne, J.M., Bauer, I., Menguy, N. and Kappler, A. (2017) Interactions between magnetite and humic substances: Redox reactions and dissolution processes. *Geochem. Trans.*, **18**, 1–12. <https://doi.org/10.1186/s12932-017-0044-1>
- Sundman, A., Vitzhum, A.-L., Adaktylos-Surber, K., Figueroa, A.I., van der Laan, G., Daus, B., Kappler, A. and Byrne, J.M. (2020) Effect of Fe-metabolizing bacteria and humic substances on magnetite nanoparticle reactivity towards arsenic and chromium. *J. Hazard. Mater.*, 121450. <https://doi.org/10.1016/j.jhazmat.2019.121450>
- Tominski, C., Heyer, H., Lösekann-Behrens, T., Behrens, S. and Kappler, A. (2018) Growth and population dynamics of the anaerobic Fe(II)-oxidizing and nitrate-reducing enrichment culture ks. *Appl. Environ. Microbiol.*, **84**, e02173–02117. <https://doi.org/10.1128/AEM.02173-17>
- Uebe, R. and Schüler, D. (2016) Magnetosome biogenesis in magnetotactic bacteria. *Nat. Rev. Microbiol.*, **14**, 621. <https://doi.org/10.1038/nrmicro.2016.99>
- Usman, M., Byrne, J., Chaudhary, A., Orsetti, S., Hanna, K., Ruby, C., Kappler, A. and Haderlein, S. (2018) Magnetite and green rust: Synthesis, properties, and environmental applications of mixed-valent iron minerals. *Chem. Rev.*, **118**, 3251–304. <https://doi.org/10.1021/acs.chemrev.7b00224>
- Wan, B., Yan, Y., Liu, F., Tan, W., Chen, X. and Feng, X. (2016) Surface adsorption and precipitation of inositol hexakisphosphate on calcite: A comparison with orthophosphate. *Chem. Geol.*, **421**, 103–11. <https://doi.org/10.1016/j.chemgeo.2015.12.004>
- Widdel, F., Schnell, S., Heising, S., Ehrenreich, A., Assmus, B. and Schink, B. (1993) Ferrous iron oxidation by anoxygenic phototrophic bacteria. *Nat.*, **362**, 834. <https://doi.org/10.1038/362834a0>
- Wilfert, P., Dugulan, A.I., Goubitz, K., Korving, L., Witkamp, G.J. and Van Loosdrecht, M.C.M. (2018) Vivianite as the main phosphate mineral in digested sewage sludge and its role for phosphate recovery. *Water Res.*, **144**, 312–21. <https://doi.org/10.1016/j.watres.2018.07.020>